PCCP

Accepted Manuscript

ROYAL SOCIETY OF CHEMISTRY

www.rsc.org/pccp

Wall embedded electrodes to modify electroosmotic flow in silica nanoslits

Harvey A. Zambrano,* Nicolás Vásquez, and Enrique Wagemann

Department of Chemical Engineering, Universidad de Concepcion, Concepcion, Chile

E-mail: harveyzambrano@udec.cl
Phone: +56 (0)41 2201468

Abstract

Electroosmotic flow in a silica slit channel with nonuniform surface charge density is investigated. In nanoconfinement, the electrical double layer occupies a non-negligible fraction of the system. Therefore, modifying the charge density on specific locations on the channel wall surface allows effective manipulation of the electroosmotic flow rates. In the present study, extensive (160 ns) nonequilibrium molecular dynamics simulations are conducted to investigate the ability to control the electroosmotic flow control in a nanoslit by patterning the surface potential. The mechanism to modify the surface charge consists of a set of charged electrodes embedded within one of the channel walls. The presence of the embedded electrodes result in the redistribution of ions in the electrolyte solution and in the alteration of the electroosmotic flow throughout the nanochannel. Indeed, the results reveal significant changes in the electroosmotic driving force and velocity profiles including local flow reversal. This study provides physical insight into the direct manipulation of the electrokinetic flow in nanoslits.

Keywords

Electroosmosis, Embedded electrodes, Silica, nanochannels, Molecular Dynamics.

*To whom correspondence should be addressed

Introduction

Fabrication techniques have evolved dramatically over the past two decades,[1–7] allowing us to conceive systems integrating fluid conduits with length scales comparable to the size of intra-cellular structures.[5,8–10] Molecular level understanding of fluid transport is a key point to open the door to mimic the highly efficient natural fluid transport processes in different technological areas.[11–14] Nevertheless, nanofluidic applications[15] present challenges to the implementation of classical fluid dynamics models due to the fact that inherent to the nanoconfinement, the extremely large surface to volume ratio and the very short time scale dominate the fluid transport[16–21] Therefore, a significant issue for design and fabrication of integrated fluidic nanosystems arises from predicting and controlling the flows throughout nanoscale conduits.

Due to the fundamental requirement of global charge neutrality, an electrolyte solution in contact with a charged surface develops an Electrical Double Layer (EDL)[22–24] that screens the net surface charge density. The EDL concept was introduced in the early works of Gouy, Debye, Chapman and Huckel.[24–27] This model dictates that the surface where hydrodynamic no-slip boundary conditions are enforced should reside near the boundary between a stagnant layer of fluid with bound ions adjacent to the solid surface known as the Stern layer, and a mobile layer containing a diffuse charge distri-

bution (diffuse layer). Indeed, if an electric field is applied parallel to the solid surface, the co- and counter ions in the diffuse layer will move as a response to the applied electric field.[22,23,28] The excess of counter ions in the diffuse layer, drag water molecules inducing a flow parallel to the solid surface known as electroosmotic flow,[23,24,29] wherein the strength of the applied electric field and the surface charge density govern the fluid transport.[22,28] Furthermore, in nanoconfined electrolyte solutions, due to the extremely large surface to volume ratio, the structure and thickness of the EDL determine significantly the electroosmotic flow rates.[20,30]

Controlling the electroosmotic flow in micro and nanoscale conduits is a key for the design of functional integrated micro and nanofluidic systems.[5,14] In the last two decades, the control of electroosmosis in microfluidic devices by applying external electric fields perpendicular to the main flow has been investigated.[31–34] Recently, nanofluidic field effect devices[35–38] feature electrodes embedded in the channel walls, have been proposed for ionic transport regulation.[37,39–41] In those devices, an externally applied potential[36,39,42] introduces a patterned surface charge distribution.[42–45] Despite these important advances, fundamental questions about the underlying physics of the fluid and ionic transport remain open.[23,24] Due to the characteristic length scale of nanofluidic channels, molecular surface roughness,[24,43] steric and hydration effects,[46,47] van der Waals and electrostatic interactions[8,20,40,48,49] can govern the overall system behavior, resulting in deviations from the macroscale fluid behavior.[16,49–54] Indeed, species distributions, local flow rates and electroosmotic velocity profiles for gated silica nanofluidic devices are still basically unknown.[20] Moreover, nanoscale effects such as the channel wall roughness, water molecular orientation near the walls and local viscosity can significantly alterate the electrokinetic transport. In this work, the electroosmotic flow of a 0.205 M KCl water solution confined in a slit-like amorphous silica nanochannel with a spatially non-uniform surface charge distribution is evaluated. We conduct all-atoms Molecular Dynamics (MD) and NonEquilibrium Molecular Dynamics (NEMD) simulations over 160 ns to elucidate flow physics in a nanoslit channel with height of ca. 7 nm featuring counter-charged electrodes embedded in the bottom wall. The electrodes inserted in the wall are physically separated from the electrolyte solution by a thin silica slab[55] of ca. 0.4 nm as shown in Figure 1.

Simulation Details

To study the electroosmotic flow, a 0.205 M KCl water solution is confined in an amorphous silica slit as shown in Figure 1. All-atoms MD and NEMD simulations are conducted using the simulation package FASTTUBE.[21,56,57] The equations of motion were solved by implementing the leapfrog algorithm with a time step of 1 fs for the simulations of silica amorphization and with a time step de 2 fs for the rest of the simulations. We use potentials previously developed for modeling silica, water and ionic species,[16,51,58] which have been calibrated using dedicated criteria. The water model is based on the simple point charge SPC/E model[59] with van der Waals interactions truncated at 1 nm.[16,51,58] The channels are filled adding sufficient water molecules to achieve the desired pressure (1 bar) at 300K. The silica is described by the TTAMm model developed by Guissani and Guillot.[60] For details of the potential we refer the reader to Zambrano et al.[16,58] To create an amorphous silica channel, cristobalite cells are replicated to build two parallel crystalline slabs, with each slab containing 7040 Silicon atoms and 14080 Oxygen atoms. An annealing procedure is implemented,[58,61] wherein, the silica slabs are coupled to a Berendsen heat bath with a time constant of 0.1 ps. The cristobalite is heated to 3000 K keeping the temperature constant during 10 ps, subsequently, quenching the system from 3000 K to 300 K by imposing a cooling rate of 70 K/ps until the equilibrium state is reached. The potassium (K) and chloride (Cl) ions are described by modeling the atoms as Lennard-Jones spheres with a partial charge placed on the center of the parti-

cle. All the ionic interactions are described employing Coulomb and Lennard-Jones potential terms with potential parameters obtained using the Lorentz-Berthelot mixing rules taking basic parameters for the individual species from Koneshan et al[62] and Zambrano et al.[58] For the Cl-Cl and K-Cl interactions, effective polarization terms to model the dipole interaction are added, which include the averaged effect of the many-body interactions, for details the reader is refered to Zambrano et al.[51] and to Walther et al.[63] Electroosmotic flow through the slit silica channel with height of c.a. 7 nm is generated by imposing axial electric fields of 0.25, 0.5, 0.75 and 1 V/nm. In fact, these fields are very high but required in the simulations to enhance signal-to-noise ratio. Certainly, the strengths of the electric fields imposed in the present study may be of concern for experimentalists however these values are in line with previous MD studies of electrolyte solution in nanochannels.[24,64] Moreover, the electric field of a water molecular near a cation is 20 V/nm therefore 20 times the highest electric field applied in the present study.

In the simulations, the channel consists of two slabs of amorphous silica with size of 34.8 nm×2.5 nm×3.4 nm representing the channel walls. The walls are aligned parallel to the x-y plane, while the height of the channel is defined along the z-axis cf. 1. The simulations are conducted in an orthorhombic box, the dimensions of the box are 34.8 nm × 2.5 nm × 28 nm, which allow for enough z-distance to avoid interactions between periodic images. Since, the amorphous silica walls are rough, we define the height of channel as the averaged distance between the deepest points on the channel walls. The channel volume is corrected by taking into account the volume of the silica roughness. The confined solution consist of 20200 water molecules, 65 chlorides and 85 potassiums. After, the amorphization of the silica walls, partial charges are modified to a value of -0.0067 e in each atom within the two outermost atomic layers of the two silica slabs to reproduce a surface charge density of -0.115 e/nm^2. We noted that a silica surface becomes electrically charged by releasing protons through complex electro-chemical reactions[65,66] therefore the surface charge of a silica surface depends on the electrolyte solution concentration and pH. Moreover, in a system with embedded electrodes, the effect of the electrodes on the surface potential depends also on parameters such as the instantaneous electrolyte concentration and the thickness of the dielectric layer separating the electrolyte solution and the electrodes.[36,55] In general, MD simulations with reacting force fields (e.g. Reax FF[67]) are very expensive in terms of computational resources, which limit the studies with reacting force fields to very small systems during relatively short times.[66,68,69] In this study, we use classical MD simulations therefore the surface charge density on the walls is assumed to be constant during the flow simulations, which is in line with previous studies.[20,64,70] Nevertheless, we realize that non-reactive MD studies have limitations thus this kind of studies should be complemented by continuum modeling studies including reactions[36] and experiments.[7,71]

Immobilizing the amorphous silica slabs, water and ions are released in the NVT ensemble at 300 K during 5 ns to ensure proper equilibration of the water and ionic species. Afterward, an axial electric field is imposed, which consists of a constant force applied on each ion in direction parallel to the x-axis. The water temperature is maintained at 300 K by applying a Berendsen heat bath to the y velocity component transverse to the main flow directions. Nevertheless, we verify that applying the heat bath to all three velocity components does not affect the computed flow. After 10 ns, two counter-charged embedded electrodes are implemented in the system. The two electrodes are simulated by modifying the point charges of specific atoms in the bottom silica wall as shown in Figure 1. In particular, on each atom within a slab portion delimited by $x > 5.0$ nm and $x < 12.9$ nm, a partial charge of -0.004 e is imposed to reproduce a charge density of -0.293 e/nm^3 in the negatively charged electrode. The charge distribution in the electrode generates a surface charge density of ca. -0.450 e/nm^2, four times higher than the surface charge density of the bare silica. Correspond-

ingly, on each atom within a slab portion delimited by x> 21.9 nm and x < 29.8 nm, a partial charge of 0.004 e is imposed to reproduce a charge density of 0.293 e/nm^3 in the positively charged electrode. We note that, the electrodes are isolated from the electrolyte solution by a thin silica layer with height of ca. 0.40 nm. In this study, the overall systems are electrically neutral. In order to compute the long range electrostatic forces, a SPME (Smooth Particle Mesh Ewald) algorithm [72] is implemented with corrections for the slab geometry.[73] In the x, y and z directions, 320, 30 and 250 reciprocal lattice vectors are used respectively, and a real space cut-off of 1 nm is implemented wherein the electrostatic interactions are computed directly. The simulations are conducted for more than 160 ns and properties are computed using trajectory data extracted from the last 60 ns. In the simulations performed to calibrate the potentials, the procedure to conduct the simulations and the methodology to compute the water contact angle were reported in Zambrano et al.[51,58] Moreover, in the present study we evaluate the presence of an charged electrode embedded within the silica substrate, hence the polarity of the embedded electrode is systematically changed and the equilibrium water contact angle is computed unsing a three-dimensional binning method.[57,58]

Results and discussion

We conducted simulations of a case with uniformly charged surfaces, imposing axial electric fields[24,53,64,74] of 0.25, 0.5, 0.75 and 1.0 V/nm. The species concentration profiles, flow rates and tangential fluid velocity (x-direction) across the channel are key quantities in the analysis of local surface effects on the electroosmotic phenomena. In this study, the atomic trajectory data are extracted each 100 fs to compute the fluid velocity, the water flow and the species concentration profile. The velocity and the concentration profiles are computed using the binning method, while the water flow is computed by following the procedure presented by Yoshida et al.[75] Figure 2 shows the electroosmotic velocity profiles as a function of the z coordinate, which is defined as the distance in the direction perpendicular to the solid-liquid interface, with $z = 0$ at the boundary of the computational box. The flow velocities in Figures 2A and 2B are averaged over the entire channel length. In Figure 2A, the velocity profiles for the different axial electric fields exhibit the expected shape for electroosmotic flows, the plug-like profile with flow velocities of 0.12, 0.4, 1.0 and 1.35 nm/ns for applied axial electric fields of 0.25, 0.5, 0.75 and 1.0 V/nm respectively. Indeed, the velocity profiles confirm a linear response of the system to increasing tangential electric fields in line with previous studies.[24,64,76] Figure 2B shows the electroosmotic velocity profiles as a function of the z coordinate for the cases with embedded electrodes. In these cases, the velocity profiles differ from the velocity profile computed for the cases with uniformly charged walls. Indeed, in Figure 2B, the velocity profiles display an assymetric shape with higher velocities near the top silica surface while lower velocities and even reversed flow velocities are observed near the bottom silica surface wherein the electrodes are embedded. The velocity profiles confirm that strong applied axial electric fields diminish the effect of the surface electrodes, as observed by Zambrano et al.,[45,51] stronger forces driving the ions in direction tangential to the surface decreases the action of the transversal electric field of the electrodes. Here, we compute maximum flow velocities of ca. 3.0, 0.75, 0.2 and 0.07 nm/ns for axial electric fields of 1, 0.75, 0.5 and 0.25 V/nm, respectively. A region with stangnant water is observed for the case with axial electric field of 0.75 V/nm. In fact, in the cases with axial electric fields of 0.25 and 0.5 V/nm, counter-flow is generated, with negative flow velocities of ca. 0.35 and 0.5 nm/ns, respectively. For these two cases we compute rates of counter-flow of 120 and 160 water molecules per nanosecond, respectively.

The Figure 3 reveal local alteration in the velocity profiles along the x coordinate direction. Specifically, Figure 3 shows the x component of the velocity computed at three particular positions along the x coordinate direction for ax-

ial applied electric fields of 0.25 (red dots), 0.5 (solid blue line) and 0.75 nm/ns (dashed black line). Indeed, the Figure 3A shows the flow velocity profile over the negatively charged electrode, the Figure 3B shows the flow velocity profile computed over the gap between the two electrodes and the Figure 3C shows the velocity profile computed on the positively charged electrode. The electroosmotic velocity for the case with applied electric field of 0.75 V/nm, depicted by the dashed black line in Figure 3, allows to analyse the influence of different surface charge on the local electroosmotic flow. Therefore, over the two negatively charged regions on the bottom wall, the flow velocity is positive, which implies that the flow is from left to right (Figures 3A and 3B) while it turns negative (right to left) on the positively charged electrode (Figure 3A). The cases with embedded electrodes and applied electric fields of 0.25 and 0.50 nm/ns show negative velocities or counter-flow on the three evaluated regions along the entire length (x-direction) of the bottom wall. Indeed, the velocity profiles in Figures 3A, 3B and 3C reveal that near the top wall, water flows in the direction of the applied electric field. Therefore, we infer the presence of vortical structures for applied electric fields of 0.25 and 0.50 nm/ns along the entire length of the channel. Furthermore, in Figure 3C for the case with a electric field of 0.75 V/nm, the flow velocity profile, computed on the positively charged electrode, displays a region with flow recirculation centered (zero velocity point) at c.a. 1.5 nm over the bottom silica surface. Nevertheless, as shown in Figure 2B, in the case with an axial electric field of 1 V/nm, a higher applied electric field not only increases the electroosmotic driving force but also removes counter and coions from the EDL resulting in a weaker effect of the patterned surface charge on the electroosmotic flow, in line with previous results.[51]

Moreover, we compute the ion concentrations and the electrokinetic driving force as functions of the z coordinate for the systems with and without embedded electrodes using a bin size of 0.18 nm. The ion concentration profiles and the electrokinetic driving force for the channel with an axial electric field of 0.50 V/nm without electrodes are shown Figures 4A and 4B. In Figure 4A, the blue solid line depicts the potassium concentration while the green dotted solid line depicts the chloride concentration. As expected in a 0.205 M KCl water solution confined inside a nanochannel with negatively charged walls, the concentration profiles reveal that the potassium ions are attracted to the walls whereas the chloride ions are rejected to the bulk. Moreover, the ion concentration profiles in Figure 4A, evidence the presence of an EDL with thickness of ca. 1.8 nm. The thickeness of the EDL is defined by the distance (z-direction) wherein the cloride and potassium concentration profiles match the bulk values. Furthermore, we compute a Debye screening length[77] of 0.6 nm, hence the EDL thinkness in the channel corresponds to three times the Debye screening length, in line with previous theoretical studies of nanoconfined KCl water solutions.[78] In Figure 4B, the electrokinetic force acting on the ions across the channel is shown for the case with axial electric field of 0.5 V/nm without embedded electrodes. The Figures 5A, 5B and 5C show the local ion concentration as function of the z-coordinate for the channel with embedded electrodes with an applied axial electric field of 0.5 V/nm. In particular, the ion concentration profiles computed over the negatively charged electrode, over the gap between the electrodes and over the positively charged electrode are shown in Figures 5A, 5B and 5C, respectively. The concentration profiles computed over the negatively charged electrode indicate that the positively charged potassiums are attracted to the surface whereas the chlorides are expelled to the bulk fluid. On the gap between the electrodes, the profiles disclose a similar trend to that shown on the negatively charged electrode but with an attenuated rejection of chlorides. Conversely, on the positively charged electrode, the concentration profiles show that the chlorides are attracted to the surface while the potassium are expelled, which results in a local electroosmotic flow in the opposite direction to the applied electric field. Indeed, the concentration profiles shown in the Figures 5A, 5B and 5C reveal that the structure of the EDL

on the bottom wall results locally distorted due to the presence of the embedded electrodes as compared to the EDL in the channel without electrodes shown in the Figure 4A. In general, in a confined electrolyte solution, the formation of an EDL lead to the appearance of a diffuse region, enriched in counterions and depleted in coions as shown in Figure 4A. If an external electric field is applied in the tangential direction to the solid surface, the induced electrical force will set the ions into motion and the moving counterions will drag the water molecules with them. The net force driving the water molecules is known as the electrokinetic driving force. In this study, the local electrokinetic driving force as a function of the z-distance from silica surface is shown in Figures 6A, 6B and 6C. In particular, the Figures 6A and 6B show a net force on the negatively charged surface in the same direction of the applied electric field, whereas the Figure 6c shows a net force in the opposite direction. Therefore, the driving force profiles evidence that the local electroosmotic flow in slit nanochannels can be controlled by implementing embedded electrodes even if the electrical double layers are not overlapped.

The orientation of the water molecules in response to the presence of charged species and external electric fields has been found to modify the viscosity of a nanoconfined electrolyte solution.[48] In this study, we compute the viscosity of the electrolyte solution following a similar procedure to the presented by Markesteijn et al.[79] Spefically, we conduct NEMD simulations of Poiseuille flow of both a 0.205 M KCl water solution in a silica channel with negatively charged walls and pure water confined in a silica channel with electrically neutral walls. Poiseuille flow is generated by applying a constant force on each water molecule confined in the channel. In order to control the temperature in the systems we connect the water to a Berendsen heat bath with the temperature calculated after removing the center-of-mass velocity.[59,80–82] The long-range electroostatic interactions are computed using a modified version of the SPME methodology[72] to include slab corrections in the z-direction.[73] A viscosity of 0.67 mPa s is obtained for pure water at 300 K, while a value of 0.70 mPa s is obtained for the 0.205 M KCl water solution at 300 K. The results indicate that for the concentration studied here, a weak effect on the viscosity due to the presence of the electrolyte is observed, which is in reasonable agreement with previous studies of the electroviscous effect in nanochannels.[83]

Furthermore, in recent studies, the surface polarity has been found to modify the wettability of a silica substrate.[19] Moreover, studies have reported that imposed electric fields modified the wetting of water solutions confined in nanopores.[8,49,51] In order to examinate if the electric field of the embedded electrodes induced wettability, we evaluate the contact angle of a water droplet placed on both a positively ($0.293\,e/nm^3$) and a negatively ($-0.293\,e/nm^3$) charged substrate. The water droplet consists of 18000 molecules mounted on a silica substrate of 37.9 nm × 37.9 nm × 3.4 nm following a similar procedure to that employed by Zambrano et al.[58] As a reference case, we compute a water contact angle of ca. 18 ° on a bare silica substrate with a surface charge density of $-0.115\,e/nm^2$. On the negatively and positively charged silica substrates, a conctact angle of ca. 14 ° is computed. The variation is lower than 5 °, which suggests that the effect of the electrodes on the wettability is negligible for the systems evaluated in this study.[19]

Recent experiments have indicated that electroosmotic flow in nanodevices can be controlled by using embedded electrodes[7,40,71] nevertheless, several fundamental questions about the underlying physics of nanoscale flow remain open. In the present atomistic study, we use a set of very high electric fields, which allow for an all-atom description of the electrokinetic phenomena to perform long time (more than 100 ns) simulations. We realize that these high electric fields are very difficult to attain in experiments however the results of the present study suggest that lower axial electric fields could be used still generating counter-flow as shown in the Figures 2 and 3. In these figures the cases with electric fields of 0.25 and 0.5 V/nm display counter flow whereas the case with highest applied electric field (1V/nm) does not display

counter flow. Indeed, with this study, we attemp to provide information that may improve the understanding of how nanoscale electroosmotic devices work and encourage more experimental work related to the fabrication and characterization of electroosmotic nanofluidic devices.

Summary and conclusions

We present an atomistic study of the electroosmotic flow in a nanoslit with height of ca. 7 nm whose surface charge density is patterned by inserting electrodes in one of the channel walls. Flow rates, concentration and velocity profiles across the channel provide evidence that electroosmotic flow can be controlled in a nanoconfined electrolyte by implementing counter-charged electrodes. These results have clear implications for nanofluidic technology. Specifically, the result confirms that in a 0.205 M KCl water solution confined in a silica nanoslit wherein the EDLs are not overlapped, counter-charged embedding electrodes with charge densities of $\pm$ 0.293 e/nm^3 induce reversed electroosmotic flow as axial electric fields lower than 0.75 V/nm are applied. The present study provides evidence that a nanochannel with embedded electrodes may work like a nanofluidic diode for controlling effectively the local flow direction in nanoconfined electrolyte solutions. Moreover, we propose that surface charged electrodes generating reversed flow can be implemented to induce mixing in nanoconfined flows wherein the Reynolds number is extremely low.[84]

Acknowledgement This research was funded in part by CONICYT through FONDECYT project no 11130559 and CONICYT scholarship no 221321041. We also thanks the partial financial support from the University of Concepcion through the REDOC program. The authors thank computational support from Ohio Supercomputer Center (OSC) and the National Institute for Computational Sciences (NICS). Furthermore, the authors wish to acknowledge professors Sherwin Singer, Chris Lorenz, Shaurya Prakash and Jens H. Walther for interesting scientific discussions.

References

1. Schasfoort, R. B. M.; Schlautmann, S.; Hendrikse, J.; van den Berg, A. Field-Effect Flow Control for Microfabricated Fluidic Networks. *Science* **1999**, *286*, 942–945.

2. Quake, S. R.; Scherer, A. From Micro- to Nanofabrication with Soft Materials. *Science* **2000**, *290*, 1536–1540.

3. Gates, B. D.; Xu, Q.; Stewart, M.; Ryan, D.; Willson, C. G.; Whitesides, G. M. New Approaches to Nanofabrication: Molding, Printing, and Other Techniques. *Chemical Reviews.* **2005**, *105*, 1171–1196.

4. Biswas, A.; Bayer, I. S.; Biris, A. S.; Wang, T.; Dervishi, E.; Faupel, F. Advances in top down and bottom up surface nanofabrication: Techniques, applications and future prospects. *Adv. Coll. Interf. Sci.* **2012**, *170*, 2–27.

5. Kovarik, M. L.; Jacobson, S. C. Attoliter-Scale Dispensing in Nanofluidic Channels. *Anal. Chem.* **2007**, *79*, 1655–1660.

6. Duan, H.; Berggren, K. K. Directed Self-Assembly at the 10,nmScale by Using Capillary Force-Induced Nanocohesion. *Nano Lett.* **2010**, *10*, 3710–3716.

7. Guan, W.; Li, S. X.; Reed, M. A. Voltage gated ion and molecule transport in engineered nanochannels: theory, fabrication and applications. *Nanotechnol.* **2014**, *25*, 122001.

8. Li, J.; Gong, X.; Lu, H.; Li, D.; Fang, H.; Zhou, R. Electrostatic gating of a nanometer water channel. *Proc. Natl. Acad. Sci. USA* **2007**, *104*, 3687–3692.

9. Sparreboom, W.; van den Berg, A.; Eijkel, J. C. T. Transport in nanofluidic systems: a review of theory and applications. *New J. Phys.* **2010**, *12*, 015004.

10. Whitby, M.; Quirke, N. Fluid flow in carbon nanotubes and nanopipes. *Nature Nanotechnol.* **2007**, *2*, 87–94.

11. Vo-Dinh, T.; Cullum, B. M.; Stokes, D. L. Nanosensors and biochips: frontiers in biomolecular diagnostics. *SAB* **2001**, *74*, 2–11.

12. Balasubramanian, K. Challenges in the use of 1D nanostructures for on-chip biosensing and diagnostics: A review. *Biosens. Bioelect.* **2010**, *26*, 1195–1204.

13. Lee, J.; Laoui, T.; Karnik, R. Nanofluidic transport governed by the liquid/vapour interface. *Nature Nanotechnol.* **2014**, *9*, 1–7.

14. Abgrall, P.; Nguyen, N. T. Nanofluidic devices and their applications. *Anal. Chem.* **2008**, *80*, 2326–2341.

15. Eijkel, J. C. T.; van den Berg, A. Nanofluidics: What is it and What Can We Expect From it? *Microfluid. Nanofluid.* **2005**, *1*, 249–267.

16. Oyarzua, E.; Walther, J. H.; Mejia, A.; Zambrano, H. A. Early regimes of water capillary flow in slit silica nanochannels. *Phys. Chem. Chem. Phys.* **2015**, *17*, 14731–14739.

17. Joly, L.; Ybert, C.; Trizac, E.; Bocquet, L. Hydrodynamics within the Electric Double Layer on Slipping Surfaces. *Phys. Rev. Lett.* **2004**, *93*, 1–4.

18. Romero-Vargas, S.; Giovambattista, N.; Aksay, I. A.; Debenedetti, P. G. Effect of Surface Polarity on the Structure and Dynamics of Water in Nanoscale Confinement. *J. Phys. Chem. B* **2009**, *113*, 1438–1446.

19. Giovambattista, N.; Debenedetti, P. G.; Rossky, P. J. Effect of Surface Polarity on Water Contact Angle and Interfacial Hydration Structure. *J. Phys. Chem. B* **2007**, *111*, 9581–9587.

20. Jin, X.; Aluru, N. R. Gated transport in nanofluidic devices. *Microfluid. Nanofluid.* **2011**, *11*, 297–306.

21. Zambrano, H. A.; Walther, J. H.; Koumoutsakos, P.; Sbalzarini, I. F. Thermophoretic Motion of Water Nanodroplets Confined Inside Carbon Nanotubes. *Nano Lett.* **2009**, *9*, 66–71.

22. Delgado, A. V.; Gonzalez-Caballero, F.; Hunter, R. J.; Koopal, L. K.; Lyklema, J. Measurement and interpretation of electrokinetic phenomena. *J. Coll. Interface Sci.* **2007**, *309*, 194–224.

23. Lyklema, J.; Rovillard, S.; ; De Coninck, J. Electrokinetics: The Properties of the Stagnant Layer Unraveled. *Langmuir* **1998**, *14*, 5659–5663.

24. Zhang, H.; Hassanali, A. A.; Shin, Y. K.; Knight, C.; Singer, S. J. The water-amorphous silica interface: Analysis of the Stern layer and surface conduction. *J. Chem. Phys.* **2011**, *134*, 024705.

25. Gouy, G. About the electric charge on the surface of an electrolyte. *J. Phys.: Theor. Appl.* **1910**, *9*, 457–468.

26. Chapman, D. L. A contribution to the theory of electrocapillarity. *Phil. Mag.* **1913**, *25*, –.

27. Debye, P.; Huckel, E. The theory of electrolytes. I. Lowering of freezing point and related phenomena. *Z. Phys.* **1923**, *24*, 185–206.

28. Lyklema, J. On the slip process in electrokinetics. *Coll. Surf. A* **1994**, *92*, 41–49.

29. Lyklema, J. Electrokinetics after Smoluchowski. *Colloids and Surfaces A: Physicochem. and Eng. Aspects* **2003**, *222*, 5–14.

30. Stein, D.; Kruithof, M.; Dekker, C. Surface-Charge-Governed Ion Transport in Nanofluidic Channels. *Phys. Rev. Lett.* **2004**, *93*, 1–4.

31. Hayes, M. A.; Ewing, A. G. Electroosmotic flow control and monitoring with an applied radial voltage for capillary zone electrophoresis. *Anal. Chem.* **1992**, *64*, 512–516.

32. Polson, N. A.; Hayes, M. A. Electroosmotic Flow Control of Fluids on a Capillary Electrophoresis Microdevice Using an Applied External Voltage. *Anal. Chem.* **2000**, *72*, 85287.

33. Kasicka, V.; Prusik, Z.; Sazelova, P.; Chiari, M.; Miksik, I.; Deyl, Z. External electric field control of electroosmotic flow in non-coated and coated fused-silica capillaries and its application for capillary electrophoretic separations of peptides. *J. Chromatogr. B.* **2000**, *741*, 43–54.

34. Sazelova, P.; Kasicka, V.; Koval, D.; Prusik, Z.; Fanali, S.; Aturki, Z. Control of EOF in CE by different ways of application of radial electric field. *Electrophoresis* **2007**, *28*, 756–766.

35. Hu, N.; Ai, Y.; Qian, S. Field effect control of electrokinetic transport in micro/nanofluidics. *Sens. Act. B : Chem.* **2012**, *161*, 1150–1167.

36. Yeh, L.-H.; Xue, S.; Joo, S. W.; Qian, S.; Hsu, J.-P. Field Effect Control of Surface Charge Property and Electroosmotic Flow in Nanofluidics. *J. Phys. Chem. C* **2012**, *116*, 4209–4216.

37. Lee, S.-H.; Lee, H.; Jin, T.; Park, S.; Yoon, B. J.; Sung, G. Y.; Kim, K.-B.; Kim, S. J. Sub-10 nm transparent all-around-gated ambipolar ionic field effect transistor. *Nanoscale* **2015**, *7*, 936–946.

38. Daiguji, H.; Oka, Y.; Shirono, K. Nanofluidic diode and bipolar transistor. *Nano Lett.* **2005**, *5*, 2274–2280.

39. Maleki, T.; Mohammadi, S.; Ziaie, B. A Nanofluidic Channel with Embedded Transverse Nanoelectrodes. *Nanotechnol.* **2009**, *20*, 1–6.

40. Karnik, R.; Fan, R.; Yue, M.; Li, D.; Yang, P.; Majumdar, A. Electrostatic Control of Ions and Molecules in Nanofluidic Transistors. *Nano Lett.* **2005**, *5*, 943–948.

41. Nam, u.-W.; Rooks, M. J.; Kim, K.-B.; Rossnagel, S. M. Ionic field effect transistors with sub-10 nm multiple nanopores. *Nano Lett.* **2009**, *9*, 2044–2048.

42. Xue, S.; Hu, N.; Qian, S. Tuning surface charge property by floating gate field effect transistor. *J. Coll. Interface Sci.* **2012**, *365*, 326–328.

43. Zembala, M. Electrokinetics of heterogeneous interfaces. *Adv. Coll. Interf. Sci.* **2004**, *112*, 59–92.

44. Adjari, A. Electro-osmosis on inhomogeneously charged surfaces. *Phys. Rev. Lett.* **1995**, *75*, 755–759.

45. Chen, L.; Conlisk, A. T. Effect of nonuniform surface potential on electroosmotic Flow at Large Applied Electric Field Strength. *Biom. Microdevices* **2009**, *11*, 251–258.

46. Marcus, Y. Effect of Ions on the Structure of Water: Structure Making and Breaking. *Chemical Reviews.* **2009**, *109*, 1346–1370.

47. Kiriukhin, M. Y.; Collins, K. D. Dynamic hydration numbers for biologically important ions. *Biophys. Chem.* **2002**, *99*, 155–168.

48. Qiao, R.; Aluru, N. R. Charge Inversion and Flow Reversal in a Nanochannel Electro-osmotic Flow. *Phys. Rev. Lett.* **2004**, *92*, 1–4.

49. Vanzo, D.; Bratko, D.; Luzar, A. Dynamic Control of Nanopore Wetting in Water and Saline Solutions under an Electric Field. *J. Phys. Chem. B* **2015**, *119*, 8890–8899.

50. Qiao, R.; Aluru, N. R. Surface-Charge-Induced Asymmetric Electrokinetic Transport in Confined Silicon Nanochannels. *Appl. Phys. Lett.* **2005**, *86*, 1–3.

51. Zambrano, H. A.; Pinti, M.; Conlisk, A. T.; Prakash, S. Electrokinetic transport in a waterchloride nanofilm in contact with a silica surface with discontinuous charged

patches. *Microfluid. Nanofluid.* **2012**, *13*, 735–747.

52. Qiao, R.; Aluru, N. R. Atypical Dependence of Electroosmotic Transport on Surface Charge in a Single-wall Carbon Nanotube. *Nano Lett.* **2003**, *3*, 1013–1017.

53. Joseph, S.; Aluru, N. R. Hierarchical multiscale simulation of electrokinetic transport in silica nanochannels a the point of zero charge. *Langmuir* **2006**, *22*, 9041–9051.

54. Lorenz, C. D.; Travesset, A. Charge inversion of divalent ionic solutions in silica channels. *Phys. Rev. E* **2007**, *75*, 061202.

55. Jin, H.; Dong, S.; Miao, M.; Liou, J. J.; Yang, C. Y. Breakdown voltage of ultrathin dielectric film subject to electrostatic discharge stress. *J. Appl. Phys.* **2011**, *110*, 1–4.

56. Walther, J. H.; Jaffe, R.; Halicioglu, T.; Koumoutsakos, P. Carbon nanotubes in water: Structural characteristics and energetics. *J. Phys. Chem. B* **2001**, *105*, 9980–9987.

57. Werder, T.; Walther, J. H.; Jaffe, R. L.; Halicioglu, T.; Koumoutsakos, P. On the water-graphite interaction for Use in MD simulations of graphite and carbon nanotubes. *J. Phys. Chem. B* **2003**, *107*, 1345–1352.

58. Zambrano, H. A.; Walther, J. H.; Jaffe, R. L. Molecular dynamics simulations of water on a hydrophilic silica surface at high air pressures. *J. Mol. Liq.* **2014**, *198*, 107–113.

59. Berendsen, H. J. C.; Grigera, J. R.; Straatsma, T. P. The missing term in effective pair potentials. *J. Phys. Chem.* **1987**, *91*, 6269–6271.

60. Guissani, Y.; Guillot, B. A numerical investigation of the liquid-vapor coexistence Curve of Silica. *J. Chem. Phys.* **1996**, *104*, 7633–7644.

61. Huff, N. T.; Demiralp, E.; Cagin, T.; Goddard, W. A. Factors Affecting Molecular Dynamics Simulated Vitreous Silica Structures. *J. Non-Crystal. Solids* **1999**, *253*, 133–142.

62. Koneshan, S.; Rasaiah, J. C.; Lynden-Bell, R. M.; Lee, S. H. Solvent structure, dynamics, and ion mobility in aqueous solutions at 25°C. *J. Phys. Chem. B* **1998**, *102*, 4193–4204.

63. Walther, J. H.; Werder, T.; Jaffe, R. L.; Gonnet, P.; Bergdorf, M.; Zimmerli, U.; Koumoutsakos, P. Water-carbon interactions III: The influence of surface and fluid impurities. *Phys. Chem. Chem. Phys.* **2004**, *6*, 1988–1995.

64. Lorenz, C. D.; Crozier, P. S.; Anderson, J. A.; Travesset, A. Molecular Dynamics of Ionic Transport and Electrokinetic Effects in Realistic Silica Channels. *J. Phys. Chem. C* **2008**, *112*, 10222–10232.

65. Mahadevan, T. S.; ; Garofalini, S. H. Dissociative Water Potential for Molecular Dynamics Simulations. *J. Phys. Chem. B* **2007**, *111*, 8919–8927.

66. Mahadevan, T. S.; Galofarini, S. H. Dissociative Chemisorption of Water onto Silica Surfaces and Formation of Hydronium Ions. *J. Phys. Chem. C* **2008**, *112*, 1507–1515.

67. van Duin, A.; Dasgupta, S.; ; Lorant, F.; Goddard III, W. ReaxFF: A Reactive Force Field for Hydrocarbons. *J. Phys. Chem. A* **2001**, *105*, 9396–9409.

68. Fogarty, J. C.; Aktulga, H. M.; Grama, A. Y.; van Duin, A. C. T.; Pandit, S. A. A Reactive Molecular Dynamics Simulation Of The Silica-Water Interface. *J. Chem. Phys.* **2010**, *132*, 1–10.

69. Liang, T.; Shin, Y. S.; Cheng, Y. T.; Yilmaz, D. E.; Vishnu, K. G.; Verners, O.; Zou, C.; Phillpot, S. R.; Sinnott, S. B.; van Duin, A. C. T. Reactive Potentials for Advanced Atomistic Simulations. *Annu. Rev. Mater. Res.* **2013**, *43*, 109–129.

70. Zhang, X. H.; Quin, A.; Ducker, W. A. Nanobubbles at the Interface between Water and a Hydrophobic Solid. *Langmuir* **2008**, *24*, 4756–4764.

71. Jiang, Z.; Stein, D. Charge regulation in nanopore ionic field-effect transistors. *Phys. Rev. E* **2011**, *83*, 1–6.

72. Essmann, U.; Perera, L.; Berkowitz, M. L.; Darden, T.; Lee, H.; Pedersen, L. G. A smooth particle mesh Ewald method. *J. Chem. Phys.* **1995**, *103*, 8577–8593.

73. Yeh, I.-C.; Berkowitz, M. L. Ewald summation for systems with slab geometry. *J. Chem. Phys.* **1999**, *111*, 3155–3162.

74. Freund, J. B. Electroosmosis in a Nanometer-Scale Channel Studied by Atomistic Simulation. *J. Comput. Phys.* **2002**, *116*, 2194–2200.

75. Yoshida, H.; Mizuno, H.; Kinjo, T.; Washizu, H.; Barrat, J. Molecular dynamics simulation of electrokinetic flow of an aqueous electrolyte solution in nanochannels. *J. Chem. Phys.* **2014**, *140*, 1–12.

76. Zhu, W. J.; Nicolai, H.; Shen, W. Z.; Sørensen, J. N. Modeling of Aerodynamically Generated Noise From Wind Turbines. *J. Solar Energy Engng.* **2005**, *127*, 517–528.

77. Bruus, H. Theoretical Microfluidics (Oxford Master Series in Physics). *Oxford University Press* **2008**, *First edition*, 1–346.

78. Schoch, R. B.; Han, J.; Renaud, P. Transport phenomena in nanofluidics. *Rev. Modern Phys.* **2008**, *80*, 839–883.

79. Markesteijn, A. P.; Hartkamp, R.; Luding, S.; Westerweel, J. A comparison of the value of viscosity for several water models using Poiseuille flow in a nano-channel. *J. Comput. Phys.* **2012**, *136*, 1–8.

80. Basconi, J. E.; Shirts, M. R. Effects of temperature control algorithms on transport properties and kinetics in molecular dynamics simulations. *J. Chem. Theory Comput.* **2013**, *9*, 2887–2899.

81. Ning, W.; Xinsheng, P.; Zhiping, X. Breakdown of fast water transport in graphene oxides. *Phys. Rev. E* **2014**, *89*, 012113.

82. Mudi, A.; Chakravarty, C. Effect of the Berendsen thermostat on the dynamical properties of water. *Mol. Phys.* **2004**, *102*, 681–685.

83. Mortensen, N. A.; Kristensen, A. Electroviscous effects in capillary filling of nanochannels. *Appl. Phys. Lett.* **2008**, *92*, 063110.

84. Wang, G. R.; Yang, F.; Zhao, W. There can be turbulence in microfluidics at low Reynolds number. *Lab on a Chip* **2014**, *14*, 1452–1458.

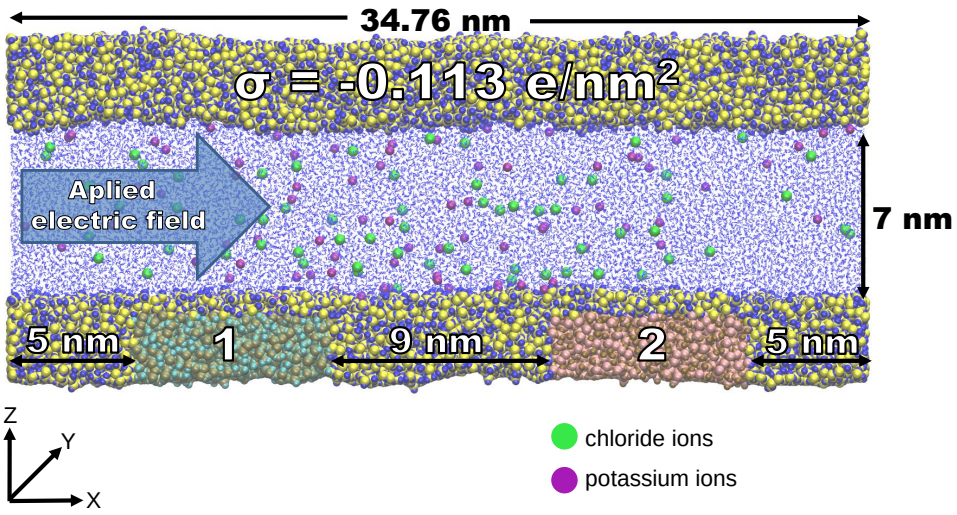

Figure 1: Electroosmotic flow of a 0.205 M KCl water solution in a nano-slit silica channel with counter-charged electrodes embedded in the bottom wall. The highlighted regions numbered 1 and 2 denote the position of the negatively and positively charged electrodes, respectively. σ denotes the charge density on the bare silica surface. External axial (x direction) electric fields with strengths between 0.25 and 1.0 V/nm are applied to the system. The height of the channel is ca. 7 nm and the system is periodic in x and y directions.

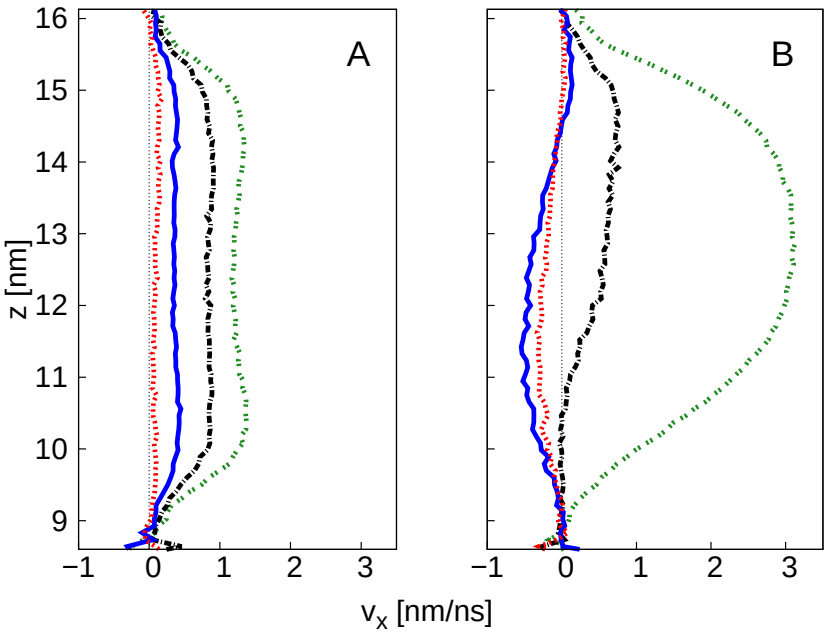

Figure 2: Electroosmotic velocity profiles in a slit channel with height of 7 nm. The reference position ($z = 0$) is located at the periodic boundary of the computational cell. The x-component velocities are computed extracting trajectories every 100 fs and averaged during the last 60 ns of the 160 ns simulation, using a bin of 34.76 nm × 2.5 nm × 0.18 nm. The vertical dashed black lines represent the zero velocity. The solid red, blue, black, and green lines depict the velocity profiles for axial electric fields of 0.25, 0.5, 0.75 and 1.0 V/nm, respectively. (A) Flow velocity profiles computed in the silica channel without embedded electrodes. (B) Flow velocity profiles computed in the channel with two counter-charged electrodes embedded in the bottom wall.

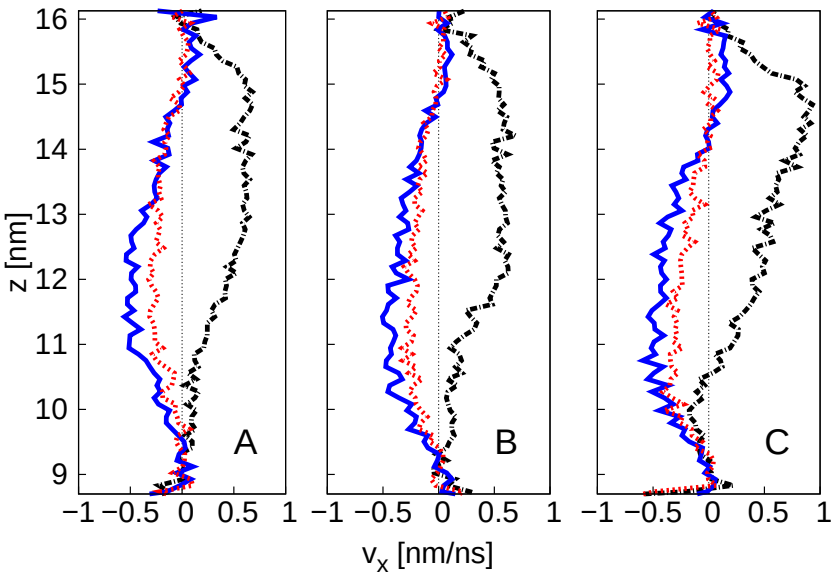

Figure 3: Electroosmotic velocity profiles across the slit channel with height of 7 nm with embedded electrodes. The profiles are computed at three locations along the x-axis direction correspoding to the negatively charged electrode, the gap between the electrodes and the positively charged electrode. The reference position ($z = 0$) is located at the periodic boundary of the computational cell. The x-component velocities are computed extracting trajectories every 100 fs and averaged during the last 60 ns of the 160 ns simulation. The vertical dashed black lines represent the zero velocity. The solid red, blue and black lines are velocity profiles for axial electric fields of 0.25, 0.5 and 0.75 V/nm respectively. (A) Flow velocity profiles computed on the negatively charged electrode. (B) Flow velocity profiles computed on the gap between the two electrodes. (C) Flow velocity profiles computed on the positively charged electrode.

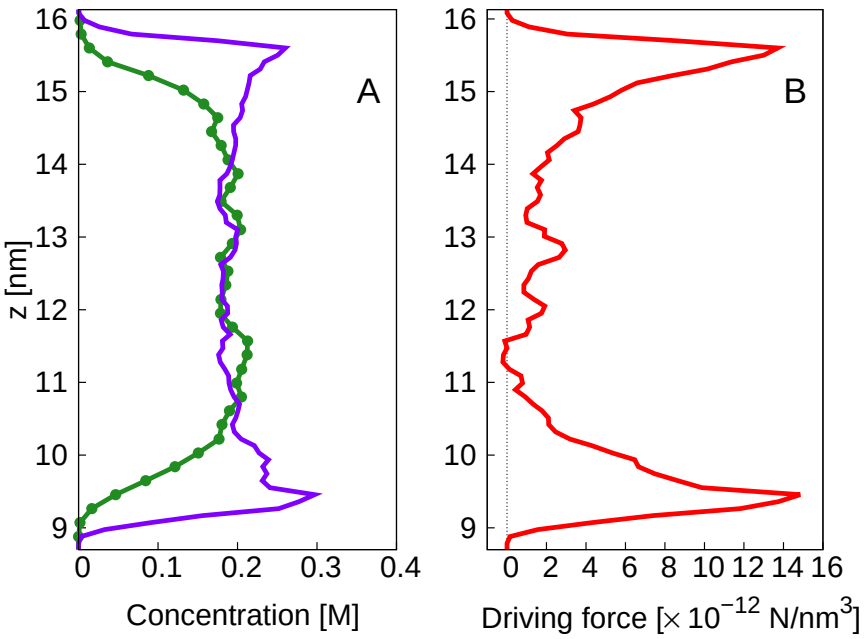

Figure 4: Ion concentration and electrokinetic driving force profiles across the slit channel with height of 7 nm without embedded electrodes for the case with an axial electric field of 0.5 V/nm. The profiles are computed along the entire length of the channel with a bin of 34.76 nm×2.5 nm×0.18 nm. The reference ($z = 0$) is located at the periodic boundary of the computational cell. (A) The dotted green line depicts the concentration of chloride ions as a function of the distance and the solid blue line depicts the concentration of potassium ions as a function of the z distance. (B) The electrokinetic driving force as a function of the z distance.

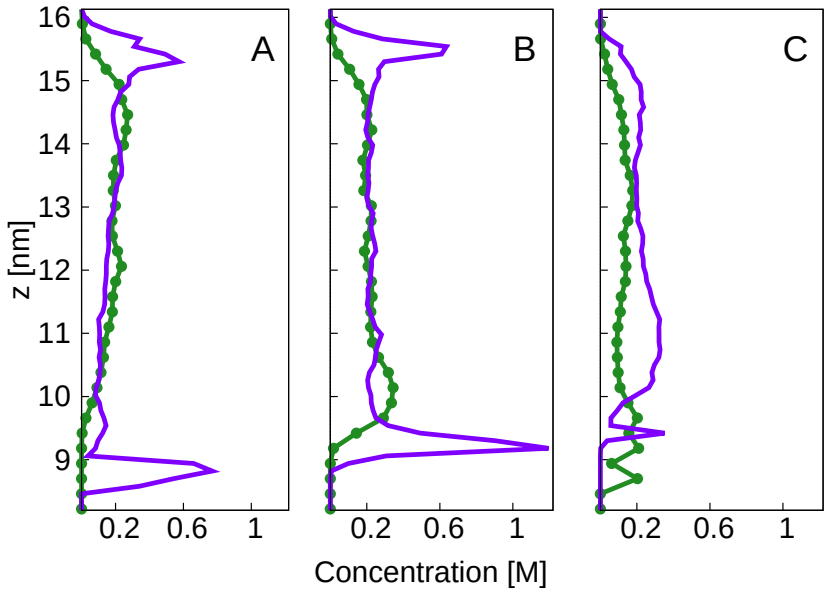

Figure 5: Ion concentration profiles across of a slit channel with height of 7 nm with counter-charged electrodes embedded in the bottom wall for the case with an axial electric field of 0.5 V/nm. The reference ($z = 0$) is located at the periodic boundary of the computational cell. The dotted green line depicts the concentration of chloride ions as a function of the z distance and the solid blue line depicts the concentration of potassium ions as a function of the z distance. (A) The ion concentration profiles computed on the negatively charged electrode. (B) The ion concentration profiles computed on the gap between the electrodes. (C) The ion concentration profiles computed on the positively charged electrode.

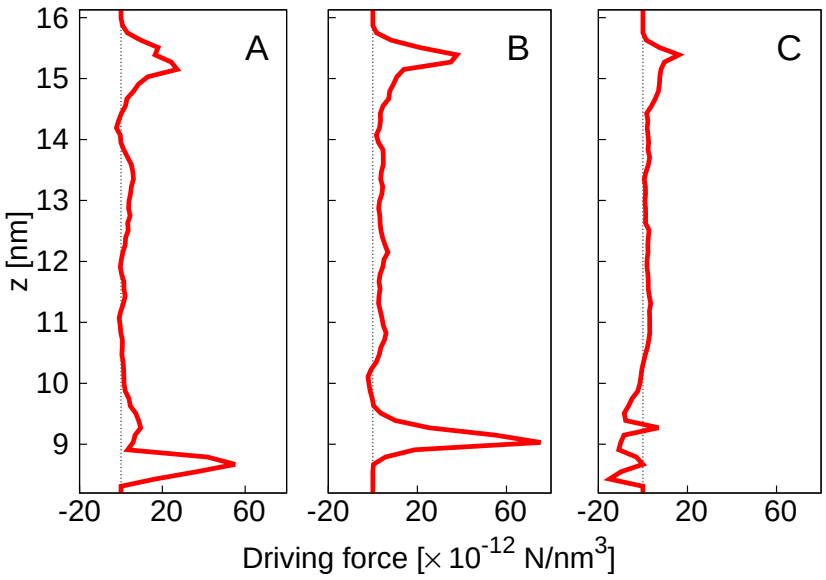

Figure 6: Electrokinetic driving force profiles across the slit channel with height of 7 nm with embedded electrodes on the bottom wall. The reference ($z = 0$) is located at the periodic boundary of the computational cell. (A) The electrokinetic driving force as a function of the z distance computed on the negatively charged electrode. (B) The electrokinetic driving force as a function of the z distance computed on the gap between the electrodes. (C) The electrokinetic driving force as a function of the z distance computed on the positively charged electrode.